

EXPERIMENTALLY DETERMINED PLASMA PARAMETERS IN A 30 CM ION ENGINE

Anita Sengupta, Dan Goebel, Dennis Fitzgerald, Al Owens
Jet Propulsion Laboratory
California Institute of Technology
Pasadena, CA
Anita.Sengupta@jpl.nasa.gov

George Tynan, Russ Dorner,
University of California San Diego
San Diego, CA

Abstract

Single planar Langmuir probes and fiber optic probes are used to concurrently measure the plasma properties and neutral density variation in a 30cm diameter ion engine discharge chamber, from the immediate vicinity of the keeper to the near grid plasma region. The fiber optic probe consists of a collimated optical fiber recessed into a double bore ceramic tube fitted with a stainless steel light-limiting window. The optical fiber probe is used to measure the emission intensity of excited neutral xenon for a small volume of plasma, at various radial and axial locations. The single Langmuir probes, are used to generate current-voltage characteristics at a total of 140 spatial locations inside the discharge chamber. Assuming a maxwellian distribution for the electron population, the Langmuir probe traces provide spatially resolved measurements of plasma potential, electron temperature, and plasma density.

Data reduction for the NSTAR TH8 and TH15 throttle points indicates an electron temperature range of 1 to 7.9 eV and an electron density range of 4×10^{10} to 1×10^{13} cm⁻³, throughout the discharge chamber, consistent with the results in the literature [1-2]. Plasma potential estimates, computed from the first derivative of the probe characteristic, indicate potential from 0.5V to 11V above the discharge voltage along the thruster centerline. These values are believed to be excessively high due to the sampling of the primary electron population along the thruster centerline. Relative neutral density profiles are also obtained with a fiber optic probe sampling photon flux from the 823.1 nm excited to ground state transition.

Plasma parameter measurements and neutral density profiles will be presented as a function of probe location and engine discharge conditions. A discussion of the measured electron energy distribution function will also be

presented, with regards to variation from pure maxwellian. It has been found that there is a distinct primary population found along the thruster centerline, which causes estimates of electron temperature, electron density, and plasma potential, to err on the high side, due this energetic population. Computation of the energy distribution function of the plasma clearly indicates the presence of primaries, whose presence become less obvious with radial distance from the main discharge plume.

Introduction

A critical wear mechanism for hollow-cathode-driven-electron-bombardment type ion engines is erosion of the discharge cathode keeper electrode due to ion bombardment from the discharge plasma. Specifically, the 30,000-hour life test of NASA's 30-cm diameter engine has found that keeper erosion is a key a life limiting mechanism due to the resultant ion bombardment of the cathode orifice plate, from the discharge plasma [4-5]. Previous work in the field has found that operational conditions that effect discharge chamber performance also can affect the extent of the keeper electrode erosion [6]. Therefore, as cathode keeper erosion and discharge chamber performance, are intrinsically linked, a detailed theoretical and empirical understanding of the plasma environment in the discharge chamber, is necessary to both improve performance and thruster life. Work in this area has been performed by Williams et al. in reference [1] using non-intrusive LIF measurements of the discharge plasma. Double Langmuir probing of an NSTAR type engine was also performed by Herman et al. [2] to characterize the radial variation in plasma properties in the conical section of the 30-cm ion engine. Work by Kolasinski et al [6] was performed to measure the rate of keeper electrode erosion as a function of discharge

operating conditions and varying the keeper to anode impedance.

The purpose of the research discussed in this paper is to characterize the plasma of the 30-cm ion engine throughout the entire discharge chamber, with the use of a high speed Langmuir probing as well as a novel optical probe technique. The focus of experimental studies performed, is to determine the plasma's sensitivity to changes in operating conditions, including cathode flow rate, main flow rate, discharge current, and cathode keeper to anode impedance changes. The probe results provide a complete mapping of the plasma in the near keeper, off axis, and cylindrical segment of the chamber.

Test Facility

All experiments were performed on a laboratory model NSTAR engine, referred to as the NKO thruster (Figure 1). This laboratory model is similar in design and performance to the NASA 30-cm diameter engine. Details on the performance comparison between NKO and the NSTAR thruster can be found in reference [6]. The thruster employs an aluminum discharge chamber, with a three-ring cusp magnetic field design. A two-grid molybdenum optics system focuses and electro-statically accelerates the ionized Xenon propellant, to produce thrust. A hollow cathode in the discharge chamber serves as the electron source. The discharge chamber is enclosed in a perforated plasma screen to prevent beam-neutralizing electrons from reaching high voltage surfaces.

The engine tests were performed in the Jet Propulsion laboratory's 3m by 10m vacuum chamber endurance test facility (Figure 2). The facility has a total pumping speed of 100 kL/s providing a base pressure of $4E-6$ Torr, with the NSTAR full power flow rates. The chamber was lined with graphite panels to reduce the amount of material back sputtered onto the engine and high-speed probe positioning system. The propellant feed system consisted of two mass flow meters for each of the cathode, neutralizer, and main lines. The downstream meters were used to measure the flow, and the upstream meters were used as flow controllers. Laboratory power supplies, capable of operating the engine over the full NSTAR throttle range, were used to run the thruster. A LABVIEW computer data acquisition system was used to record engine electrical parameters and control the flow meters.

The engine was configured to allow the translation of 7 probes providing radial profiles from the anode wall to just past the thruster centerline for both the cylindrical and conical chamber segments. The probe locations provided a spatially resolved discharge plasma characterization, starting from 1cm downstream of the discharge cathode keeper up to and including 2cm from the upstream side of the screen grid (14cm downstream of the keeper). The axial locations of the probes were 1,2,3,4,6,10, and 14 cm downstream of the keeper electrode. Emphasis was on the near keeper plasma to provide sufficient axial resolution in the region believed to be the source of high-energy ions responsible for the previously observed cathode keeper erosion.[3-5]

The probes were inserted into and retracted from the discharge chamber by a high speed linear translation stage (Figure 5b). A Kollmorgen brushless servomotor in conjunction with a Servostar CD driver, was used to drive a Velmex lead screw stage. The computer controllable motor was able to operate at a variety of speeds, with a maximum speed of 50.8 cm/sec. This enabled a full probe insertion and retraction operation to be less than 0.8 sec. A sample translation profile is shown in figure 6b. The stage was fitted with a home switch and two limit switches to bring the stage back to the same starting point and prevent operation outside of the desired range. Position was recorded with a linear position transducer, which is essentially the voltage output of a voltage divider.

The probes were mounted to the stage on the probe mount shown in figure 4a. Teflon spacers and setscrews were used to hold the alumina tubes in a fixed position on the probe mount. Alignment and insertion into the engine was accomplished by a thruster probe mount, which houses each probe in stainless steel collars inserted into the anode wall that protrude up to 0.76 cm into the discharge chamber (Figure 4b and 5a). Precision alignment of the system was accomplished via fine adjustment screws on both the probe mount and thruster probe mount.

During each translation, a combination of single langmuir probes and optical probes translated into the discharge chamber. Each langmuir probe consisted of a thoriated tungsten cylindrical rod spot welded to a stainless steel wire that was fed through either a single or double bore alumina tube with an OD of 0.48 or 0.51 cm respectively. Each Tungsten rod extended 0.6 to 0.64 cm beyond the ceramic. The stainless steel wire extended 15 to 20 cm beyond

the ceramic and was fitted with coax connection to electrically connect each probe to the junction box (Figure 4a). The position of the wire was maintained with several layers of high temperature shrink tubing placed at the end of the rod. Probe diameters of 0.1 cm and 0.15 cm were used primarily to investigate the effect of varying the effective sheath to probe radius on plasma parameter measurement consistency, and limitations of the use of OML theory data analysis in low-density plasmas [7-10]. Each probe coax output connection was fed into a shielded junction box (Figure 4a). The junction box could take up to 5 probe electrical connections. The 5 output signals from the junction box were routed through the vacuum chamber to 2 ISI SHV10 high voltage vacuum feedthrus. The vacuum feedthrus and the air-side cabling were shielded to facility ground to reduce signal noise.

The optical probe was modeled after a technique developed in references [11,12]. Each optical probe consisted of a 0.48 NA optical fiber fed through a 0.51 cm OD alumina rod. The optical fiber, purchased from Thor labs, was chosen for its large aperture size and sensitivity to the visible near-IR range. The fiber consists of a quartz cylinder surrounded by silicon cladding. As an optical fiber can see light in all directions, it was necessary to limit the light it saw to a small volume of plasma at the probe tip location. This was accomplished by inserting into the alumina tube, a thin walled stainless tube with a 2cm by 1 cm window cut into it with a solid cap spot welded to the end. The optical fiber was then fed into the stainless tube, and recessed 1cm from the window. The stainless steel tube was aligned such that the window extended just beyond the alumina housing, only allowing light from the window into the optical path of the fiber optic. In order to minimize the effect of reflections from photons not in the plasma volume of interest, the optical probe was inserted into the plasma several times, allowing deposition of a low reflectivity coating on and in the exposed stainless steel tube. The light from each fiber optic was passed through a tunable spectrometer. The output of the spectrometer was received by a high sensitivity photomultiplier tube module. Due to the high sensitivity of the PMT, it was necessary to house it in a light tight box fitted with a computer programmable shutter. The electronic shutter allowed minimum exposure to light and high precision exposure times from as low as 6 ms.

A separate LABVIEW data acquisition system was used to control the translation stage, electronic shutter, probe power supplies, and record current/voltage data. A high-speed data acquisition card, with a sampling rate of up to 2 MHz for analog input and 1kHz for analog output was used to record current-voltage waveform data, linear position output, PMT output, and provide control voltages for the bias power supply, electronic shutter, and high-speed stage. A bipolar power supply was used to bias the Langmuir probes +/- 50V with respect to cathode common. The voltage waveform was a saw tooth ramp, cycled at 100 Hz typically for a duration of 1 second. The bias supply was placed in series with the probe and cathode common, and allowed to float at the thruster potential with respect to ground. As the data acquisition system was at ground potential, and the thruster operating up to 1250 V above ground potential, it was necessary to isolate the probe signal and control voltage for the bias power supply. This was accomplished via the use of two fiber optic link modules. The fiber optic link modules consisted of a separate transmitter and receiver module, each end receiving and transmitting 0-5 V respectively. The current through each probe was measured across a 2-Ohm current shunt. The voltage output from the shunt was conditioned using a low-pass RC filter circuit, and then routed through the fiber optic link module, to be read by the grounded data acquisition system. The control voltage for the bias supply was transmitted in the reverse manner from ground to high voltage through the fiber optic link module.

Results and Discussion

Test Matrix

The discharge plasma was characterized by langmuir and optical probes at the NSTAR TH15 and TH8 throttle points. Table 1 is the NSTAR throttle table from reference [5]. Previous ground test data indicate these throttle points result in significant erosion of the keeper electrode by ion bombardment from the discharge plasma [4,5]. It has been suggested, in the literature, that the operating conditions and or impedance between the cathode keeper electrode to the anode, may reduce or eliminate the ion bombardment. Therefore, characterizing the discharge plasma as a function of these operational changes may then shed light onto the physics behind the bombardment mechanism. A test matrix was generated to determine the

discharge plasma's sensitivity to variations in cathode flow rate, main flow rate, discharge current, and the impedance between cathode keeper and anode. The cathode flow rates were varied at +/- 10% and +/- 20% from the nominal set point. Main flow rate was varied +/- 10% from the nominal set point. Discharge current was varied +/- 0.5 A from the nominal set point. For each nominal operating point, the discharge current was set manually, to match the throttle table beam current set point. Therefore, for experiments that varied either the cathode or main flow rate from nominal, the nominal discharge current setting remained the same, and the beam current and discharge voltage varied accordingly.

Varying the cathode keeper to anode impedance was also investigated at 1kOhm and 100 Ohm's, at the nominal set points only. Kolasinski et. al [6] determined that varying this impedance resulted in a 20% decrease in the erosion of the keeper electrode. Therefore understanding the differences in plasma potential and density under these two conditions is critical to developing analytical approaches to model these effects.

Data Reduction

The data obtained from each probe translation consists of current voltage characteristics for each probe, at 20 to 25 radial locations for each translation. As any probe inserted into a plasma will by its very nature disturb the plasma, a translation time of less than 0.8 seconds was used. Only data from the in-sweep was analyzed, to reduce errors due to probe insertion plasma disturbances. As the probe was swept into the discharge plasma, the bias voltage was swept from -50 to +50V, with respect to cathode common, at 100 cycles per second. With a probe translation speed of 50 cm/s, this resulted in a spatial resolution of 0.13 cm per probe characteristic. A typical probe characteristic is shown in figure 6a. The exponential portion of the curve, commonly called the electron saturation or retardation region of the characteristic, was used to determine the electron temperature, electron number density, and plasma potential. A maxwellian velocity distribution was assumed, for the simplicity of analysis, and Chen's method for obtaining electron temperature was used [8,14]. A linear curve fit was applied to the natural log of the electron saturation region of each trace using the software IGOR. The

reciprocal of the resultant linear slope is the electron temperature at the particular axial and radial location in units of electron volts. The plasma potential was calculated from the methodology discussed in reference [7], where the plasma potential may be obtained from the inflection point of the first derivative of the probe current with respect to the bias voltage. The first derivative of the probe current was calculated using a forward difference routine, and the voltage corresponding to the maximum was defined as the plasma potential. This method was chosen as it provided the most consistent and definitive approach for all the probe traces taken and analyzed. Although the approach provides consistency, it tends to yield a higher value of the plasma potential than traditional semi-log linear extrapolations, due to the sampling of both the primary and maxwellian electron populations.

The electron number density, or plasma density, was calculated from the electron saturation current, defined as the probe collected current at the plasma potential, as defined above. Equation (1) relates the probe current, probe area, electron temperature, and plasma density, assuming a maxwellian plasma.

$$I_{sat} = \frac{1}{4} e n_e A_p \sqrt{8kT_e/\pi m} \quad (1)$$

Relative neutral density profiles were obtained from reduction of the PMT current output. The rate of production of excited neutral Xenon atoms from the ground state to state j is defined in equation (2).

$$J_j = \langle \sigma_j v \rangle e n_e n_0 \quad (2)$$

With knowledge of the flux of excited state j neutrals, the electron number density and the neutral excitation cross-section to state j, one can obtain the neutral number density. The 823.1 nm transition was chosen for these experiments, as the cross section dependence as a function of energy is known and documented in reference [14], and it does not coincide with any Xe+ or Xe++ excitation lines. In addition the signal strength for this transition is strong, and assuming optically thin plasma, the cross section for re-absorption of released photons from the transition can be assumed to be negligible and relatively constant over the range of electron temperatures investigated. With the spectrometer tuned to the 823.1 nm line, the output of the PMT is proportional to the excited neutral Xenon flux. Using T_e and n_e obtained from the

Langmuir probe traces and the PMT voltage output, variation in neutral number density can be obtained relative to other locations radially and axially in the discharge plasma.

Only preliminary proof of concept results are included in this paper for the optical probe diagnostic. Future work on this diagnostic approach will include an absolute calibration of the fiber optic system, allowing us to relate current from the PMT to a known photon flux. With this calibration, absolute number density variations will be obtained at a future date.

TH15 Studies

TH15 is the full power point, for the NSTAR thruster, corresponding to 3.6 sccm cathode flow rate, 23.4 sccm main flow rate, and 1.76A of beam current. All experiments were run with beam extraction, corresponding to a screen grid potential of 1100 V and an accelerator grid potential of -250V. Langmuir probe measurements encompassed an axial expanse of 1.1cm to 10.2 cm downstream of the keeper, and a radial expanse from the anode wall to just past the thruster centerline in both the conical and cylindrical segments. Data reduction of probe IV characteristics at the nominal TH15 operating point indicates a centerline axial variation in electron temperature from 7.9 to 4eV. Radial variation, in the conical segment spanned 7.9 to 1eV, with the maximum on the centerline, and minimum recorded at 1cm from the anode wall. Radial variation, in the cylindrical segment, spanned from 6.6 eV to 1.5eV. Electron number density was found to vary from a minimum of $1.1 \times 10^{11} \text{ cm}^{-3}$ at the anode wall, 10.2 cm downstream of the keeper, to $1.3 \times 10^{13} \text{ cm}^{-3}$ along the thruster centerline, 1cm downstream of the keeper. Plasma potential was measured with respect to cathode common, and reached a maximum of 11V above the anode potential at the exit to the keeper, and a minimum of 1.7V above the anode potential in the conical segment near the anode wall.

As mentioned previously spatial and quantitative sensitivity of the plasma parameters to changes in operating conditions was investigated. The first set of experiments performed investigated the effect of changing the cathode flow rate +/-20% from the nominal set point. As discharge voltage and double ion production are highly sensitive to cathode flow rate, it is desired determine the axial and radial variation of the electron temperature, electron density, and plasma potential in the ion engine

discharge chamber. Figures 7 through 12 are contour plots of electron number density, electron temperature, and plasma potential for the nominal and -20% reduction in cathode flow rate case. Figures 13a,b,c, are centerline variations of the plasma parameters as a function of axial distance from the keeper presented for obvious inspection of observed trends. Results indicate lowering the cathode flow reduces the centerline electron density on the order of 10% from 2 to 4 cm downstream of the keeper, as well as 1cm radially from the keeper orifice, relative to the nominal set point. Off axis however, this trend is reversed, and the 20% reduction in cathode flow rate results in a 10 to 30% increase in electron density from 2 to 5cm downstream of and 1 to 6 cm radially from, the keeper orifice. The peak electron number density was measured at 1.1 cm downstream of the keeper, along the centerline, with a magnitude of $1 \times 10^{13} \text{ cm}^{-3}$, for both the nominal and -20% reduction case. Decreasing the cathode flow rate tended to increase the peak electron temperature along the centerline and move its location axially downstream from the keeper. The nominal case peak electron temperature measured was 7.6 eV, located at the first probe position, 1cm from the keeper. Decreasing the cathode flow rate by 20% resulted in a peak electron temperature of 8.7eV, 4cm from the keeper. The flow rate reduction had a direct effect on the centerline T_e profile, but negligible effect on the electron temperature variation of axis. Decreasing the cathode flow rate significantly increased the plasma potential from 1 to 4 cm downstream of the keeper, and across the chamber radius. Along the centerline line, the plasma potential increased by as much as 30%, with respect to the nominal potential. Further analysis of the centerline plasma potential profile for the two cases investigated indicates that the nominal potential profile exhibits a jump in potential, on the order of the electron temperature at 4cm downstream of the keeper, whereas the -20% cathode flow case exhibits a relatively smooth plasma potential profile. This structure may be indicative of a double layer, which would suggest that increasing cathode flow tends to move the double layer downstream from the keeper. In the case of the -20% flow rate reduction, the double layer is not apparent, and is likely to be at the keeper orifice entrance. It is important to note, that the plasma potentials recorded in these studies, are questionably high in magnitude, suggesting that the non-maxwellian nature of the discharge plasma may introduce significant

errors into the calculation of the plasma parameters close to the centerline. Therefore magnitudes of centerline potentials, electron temperature, and plasma density have an uncertainty of as much as +30%.

Variation of the main flow rate, +/- 10% from the nominal operating point was also investigated. The centerline profiles comparing nominal and +10% nominal main flow at TH15 are found in figures 14a,b,c. Electron density calculations indicate that increasing the main flow rate resulted in a 10% decrease in the near keeper electron density, but a substantial increase from 8 to 10 cm downstream of the keeper. An increase on the order of 20% was recorded at 10cm downstream of the keeper. This spatial variation is consistent with the location at which the main flow is introduced into the chamber. Increasing the main flow rate tended to decrease the centerline electron temperature, up to 0.8eV, from the nominal case, with the most significant reduction at 10 cm downstream of the keeper. Radial variation in electron temperature profiles, tended to be less peaked and up to 0.6 eV lower in magnitude than the nominal case. Centerline plasma potentials were also reduced from 4 to 5V due to the increase in main flow rate. Radial variation in plasma potential was less peaked for the +10% main flow rate case, and significantly lower near the keeper.

Variation of the discharge current rate, +/- 0.5A from the nominal 15A was also investigated. Figures 15a,b,c show the centerline variation of the plasma parameters for the discharge current studies. As can be seen, varying the discharge current by +/-3% resulted in a slight increase in electron density, at 4cm downstream of the keeper, but little variation elsewhere. The centerline electron temperature profile for the discharge current variation studies has an unusual structure. There is a minima at 2cm and at 5cm downstream of the keeper. At the maxima, the +0.5A case T_e is 0.6eV higher than the -0.5A case. From 6 to 10 cm the electron temperature for the -0.5A case decreases at a faster rate, and at 10cm is 0.5 eV lower than the +0.5A case. The centerline plasma potential profile for the +0.5A case also exhibits an unusual structure, with a jump in potential on the order of the electron temperature at 4cm downstream of the keeper. This plasma potential profile may also be due to the presence of a double layer. In this case decreasing the discharge current tends to move the double layer downstream of the keeper, manifesting itself as a jump in the plasma potential. The -0.5A case

does not exhibit this discontinuity, suggested that if present, the double layer is upstream of the first probe location. The +/-3% variation in discharge current resulted in a plasma potentials 2 to 11eV above the anode potential, along the thruster centerline.

Radial variations in the plasma parameters due to the discharge current variation were less pronounced than those on the centerline. Reducing the discharge current tended to produce a less peaked electron temperature and electron density profile.

TH8 Studies

TH8 is the half power point, for the NSTAR thruster, corresponding to 2.47 sccm cathode flow rate, 14.4 sccm main flow rate, and 1.1A of beam current. All TH8 experiments were run with beam extraction, corresponding to a screen grid potential of 1100 V and an accelerator grid potential of -180V. Langmuir probe measurements were also made from 1.1cm to 10.2 cm downstream of the keeper, encompassing the region from the anode wall to just past the thruster centerline, for the conical and cylindrical segments of the chamber. The TH8 operating point exhibited a centerline axial variation in electron temperature from 7.2 to 5.1eV. Radial variation, in the conical segment spanned 7.2 to 0.9eV, with the maximum on the centerline, and minimum recorded at 1cm from the anode wall. Radial variation, in the cylindrical segment, spanned from 6.1 eV to 1eV. Electron number density was found to vary from a minimum of $4.1 \times 10^{10} \text{ cm}^{-3}$ at the anode wall, 10.2 cm downstream of the keeper to $1.1 \times 10^{13} \text{ cm}^{-3}$ along the thruster centerline, 1.1cm downstream of the keeper. Plasma potential was measured with respect to cathode common, and reached a maximum of 4V above the anode potential at the exit to the keeper, and a minimum of 0.5V above the anode potential in the conical segment near the anode wall. Larger plasma potentials, up to 11 V above the anode potential, were measured 6cm downstream of the keeper for nominal TH8 operation.

The spatial sensitivity of the plasma parameters to cathode flow rate was also investigated at the TH8 point. Figures 16 through 21 are contour plots of electron density, electron temperature, and plasma potential variation with radial and axial position for the nominal TH8 operating point and with -20% cathode flow rate. As with the TH15 cathode flow rate studies, decreasing the cathode flow decreases the

centerline electron density, but tends to increase it off axis, resulting in a less peaked radial distribution as compared to the nominal TH8 operating point. Figure 22a is the electron density centerline profile comparison. Decreasing the cathode resulted in a 20% reduction in plasma density from 1 cm out to 6cm downstream of the keeper. From 6cm to 10 cm, the plasma density variation reduced to zero. Figure 22b is a plot of electron temperature variation for the TH8 flow rate comparison. It can be seen that reducing the cathode flow rate has an enormous effect on the electron temperature. At 6cm downstream of the keeper the nominal electron temperature is 6 eV, as compared to 9eV for the -20% reduction in cathode flow rate case. From 6 to 10 cm downstream of the keeper, the electron temperature for the nominal case increases linearly where as for the -20% case, T_e decreases linearly. Assuming a linear trend, the T_e profiles become equal at approximately 11cm. Figure 22c is the centerline plasma potential for the two TH8 cases investigated. Both profiles exhibit a jump in plasma potential, consistent with the TH15 plasma potential structure discussed previously. The discontinuities occur at approximately the same location however, 5 cm downstream of the cathode keeper. Unlike the TH15 studies, the location of the continuity is not dependent on the cathode flow rate change for TH8. The magnitude of the increase does appear to be dependant of the flow rate setting however. The nominal TH8 case exhibited an increase in plasma potential on the order of 4eV, as compared to a 7eV increase for the -20% cathode flow rate case.

Cathode Keeper to Anode Impedance change

The final sensitivity study performed was on the variation in plasma parameters due to changing the impedance between cathode keeper and anode. Kolasinki et. al. [6] determined that the extent of erosion of the keeper electrode is dependent on the value of the impedance between cathode keeper and anode. Specifically they determined that changing the nominal impedance from 1000 Ohms to 100 Ohms, will reduce the erosion of the keeper by 20% at the TH15 operating point. Reduction of this impedance essentially reduces the voltage drop between cathode keeper and anode, and therefore the voltage difference between discharge chamber ions and the cathode keeper. A

reduction in electric field strength between the discharge plasma ions and keeper electrode should result in less sputtering of the electrode. It is therefore of interest to characterize the plasma environment as a function of this impedance.

Four cases were investigated for this set of studies, 1000 Ohms (nominal) and 100 Ohms, between cathode keeper and anode, and at the nominal TH15 and TH8 operating points. Four of the five probes were placed in the near keeper region, to obtain better resolution from 1.1 to 4.2 cm, at the expense of downstream data. The fifth probe was placed at 14 cm downstream of the keeper, however, to obtain a measurement in the near screen grid region. 0.15 cm diameter cylindrical probes were used for these studies, to minimize the Debye sheath to probe radius ratio, thereby simplifying plasma parameter calculations, albeit at the expense of increased disturbances to the plasma.

Figure 23a is a plot of the cathode keeper to common potential for the cases investigated. As can be seen, decreasing the impedance from 1000 to 100 Ohms, increases the potential by about 4V and 2V for TH8 and TH15 respectively. Figure 23b is a plot of the associated discharge loss or power required to create an ampere of beam current. As can be seen, increasing the cathode keeper voltage results in a higher discharge loss, which is essentially a reduction in efficiency. Therefore there is a trade between the keeper erosion and engine ionization performance for this operational change.

Figure 24a is the centerline electron density for the TH8 cases investigated. Reducing the impedance between keeper to anode reduces the electron density by as much as 25% from 1 to 2.5 cm downstream of the keeper. From 2.5 to 3.5 cm downstream however, the densities equilibrate, and from 3.5 to 4cm the 100 Ohm case density tend to be higher than the 1000 Ohm case. Figure 24b is the centerline electron temperature for the TH8 impedance studies. The 100 Ohm case has a 1 to 2 eV lower electron temperature than the 1000 Ohm case, from 1 to 4 cm downstream of the keeper, with the variation increasing with distance from the keeper. Figure 24c indicates the plasma potential is up to 4V higher for the 100 Ohm case, from 1 to 2.5 cm downstream of the keeper. From 2.5 to 4cm, the plasma potentials for both cases approach each other. It should also be note that the jump in the plasma potential is shifted 1cm further downstream, for the 100 Ohm case as compared

to the 1000 Ohm nominal case. Therefore, if this is a double layer structure, its axial location is directly affected by the impedance between cathode keeper to anode.

Figures 25a,b,c are plots of centerline electron density, electron temperature, and plasma potential, for the TH15 case studies. The results are notably different than the TH8 studies described above. Reducing the impedance between keeper and anode only reduced the electron density by 10% at 1cm downstream of the keeper. From 2 to 3.5 cm, the 100 Ohm case electron density was either equal to or greater than the nominal case. Similarly, the 100 Ohm case electron temperature was equivalent to the nominal case from 1 to 2.5 cm. The centerline T_e was 0.5 eV higher than the nominal case at 3cm, and lower by about 1 eV at 4 cm. The centerline plasma potential profiles were also very similar, in magnitude, and shape, up to about 2cm. At about 2.5 cm, both cases exhibited an increase in plasma potential, with the 100 Ohm case exhibiting a faster rate and magnitude of increase.

Based on the limited studies performed, reducing the impedance from 1000 to 100 Ohms at TH15 had only a minor effect on the measured plasma parameters in the near cathode region. This was not the case for the TH8 investigations. Reducing the impedance at the TH8 operating point resulted in a reduction in electron temperature and electron number density, but increase in plasma potential, in the region 1 to 3 cm downstream of the keeper. In addition, the apparent double layer structure was shifted 1cm downstream from the nominal location with the reduced impedance between cathode keeper to anode.

Electron Energy Distribution Function

All analyses performed in this paper have assumed a maxwellian distribution function for the electron population. Although reasonable estimates of the plasma parameters have been obtained, is it still a gross oversimplification of the plasma in an ion engine utilizing a hollow cathode. In fact, there is a distinct primary population in the plasma, mainly constrained to the thruster centerline, coming from the hollow cathode. It is only off-centerline that electrons on the whole tend to become thermalized, and exhibit a maxwellian distribution.

In order to qualitatively understand the nature of the distribution, the method discussed in reference [7] was used to extract the shape of the

electron energy distribution from the probe characteristics. The EEDF is proportional to the second derivative of the retarding region of the probe characteristic. If the distribution were maxwellian, one would expect to see a single peak in the second derivative corresponding to the most probable energy. A forward difference routine was used to calculate the second derivative of several probe characteristics, in order to see the structure of the probability distribution function. Figure 26 is a plot of the second derivative of two TH15 probe traces, both located 4cm downstream of the cathode keeper, but one on the thruster centerline, and the other 3cm off the centerline. As can be seen for the centerline case, there are two distinct peaks. These peaks likely correspond to a thermalized electron population at 29V and a primary electron population at 35V. The solid curve in figure 26 corresponds to the second derivative of at the same axial location but 3 cm from the centerline. Here we only see one distinct peak at 28V, consistent with a single thermalized population of electrons. These two simple examples clearly indicate the non-maxwellian nature of the discharge plasma in an ion engine. Therefore, although we have presented calculations of the plasma parameters, they are only estimates, due to the non-maxwellian nature of the plasma.

Future work in this area will include the computation of the actual EEDF as a function of axial and radial location. Using these EEDF's, more accurate calculations of electron density and temperature will be made, by integrating over the respective distributions.

Conclusions

The discharge plasma of the 30-cm-diameter NKO engine has been characterized using single langmuir probes axially from 1 to 14 cm downstream of the discharge keeper, and radially from the anode wall to just past the thruster centerline. Bulk plasma properties at both the TH8 and TH15 power points indicate electron densities and temperatures in the range of $1E11$ to $1E13$ cm⁻³ and 0.9 to 7.9 eV respectively. Sensitivity studies indicate that the plasma potential and maxwellian averaged electron temperature and density are highly sensitive to changes in cathode flow rate, and less sensitive to changes in main flow rate. In addition, plasma potential profiles indicate the existence of a double layer at both the TH15 and

TH8 nominal operating points that tends to shift upstream with reduction in cathode flow or increase in discharge current.

The discharge plasma was also characterized as a function of the resistance between cathode keeper to anode, for the TH15 and TH8 nominal operating points. The TH8 set point was found to be highly sensitive to the 1000 to 100 Ohm impedance reduction, exhibiting a lower electron density and temperature than the nominal case. Reducing the impedance also tended to raise the plasma potential and shift further downstream, the apparent double layer location at TH8. TH15 exhibited little change due to reducing the impedance from 1000 to 100 ohms. Centerline density and electron temperatures were essentially unchanged.

Overall, reducing the resistance reduces the centerline electron temperature and plasma potential, and tends to create a more uniform plasma in the radial direction, with uniformity increasing as you move towards the grid plane.

Calculation of the electron energy distribution functions from the probe traces at TH15, clearly indicate the presence of two distinct electron populations along the thruster centerline. Off axis, there appears to be only single a thermalized electron population. This finding therefore limits the accuracy of the plasma parameter calculations made on axis due to the over simplification of using a maxwellian distribution to determine density and electron temperature.

Acknowledgements

The research described in this paper was carried out at the Jet Propulsion Laboratory, California Institute of Technology, under a contract with the National Aeronautics and Space Administration.

References

- [1] Williams, G. J., et al., "Characterization of Discharge Cathode Plume," IEPC Paper, 27th International Electric Propulsion Conference, Pasadena, CA, Oct. 2001.
- [2] Herman, D., et al., "Comparison of Discharge Plasma Parameters in a 30-cm NSTAR Type Ion Engine with and without Beam Extraction", AIAA-03-5162, July, 2003.
- [3] Williams, G. J., et al., "Characterization of FMT-2 Discharge Cathode Plume," IEPC Paper #99-104, 26th International Electric Propulsion Conference, Ketakiushu, Japan, Oct. 1999.
- [4] Polk, J. E., et al., "An Overview of the Results from an 8200 Hour Wear Test of the NSTAR Ion Thruster," AIAA-99-2446, June 1999.
- [5] Sengupta, A., et al., "Status of the Extended Life Test of the Deep Space 1 Flight Spare Ion Engine After 30,352 Hours of Operation," AIAA-2003-4558, July 2003.
- [6] Kolasinski, R. D., and Polk, J. E., "Characterization Of Cathode Keeper Wear By Surface Layer Activation," AIAA-2003-5144, July, 2003.
- [7] Godyak, R.B., et. al., "Probe Diagnostics of Non-maxwellian plasmas", J. Applied Phys., 73 (8), 15 April 1998.
- [8] Sudit, I.D., Woods, R.C., "A study of the Accuracy of Various Langmuir Probe Theories", J. Appl. Phys. 76 (8) 1995.
- [9] Clements, R.M., "Plasma Diagnostics With Electric Probes", J. Vac. Sci. Technol., 15 (2), April 1978.
- [10] Laframboise, J.G., "Theory of Spherical and Cylindrical Langmuir Probes in a Collisionless, Maxwellian Plasma At Rest", UTIAS Report No. 100, June 1966.
- [11] Yun, S., et. al., "Neutral Uniformity and Transport mechanisms for Plasma Etching", Physics of Plasmas, (8) 6, June 2001.
- [12] Yun, S., et. al., "Measurement of radial neutral pressure and plasma density profiles in various plasma conditions in large-area high-density plasma sources", Physics of Plasma, (7) 8, August 2000.
- [13] Goebel, D.M., et. al., "Hollow Cathode and Keeper-Region Plasma Measurements Using Ultra-Fast Miniature Scanning Probes", Joint Propulsion Conference, Fort Lauderdale FL, July 10th -13th, 2004
- [14] Chen, F.F., "Plasma Diagnostic Techniques", Ch 4.
- [15] Chen, F.F., "Introduction to Plasma Physics and Controlled Fusion", Second Edition, Plenum Press, New York, 1984.
- [16] Feltsan, R.V., et. al., I.P., Ukr., Fiz. Zh., (13) 205, 1968.

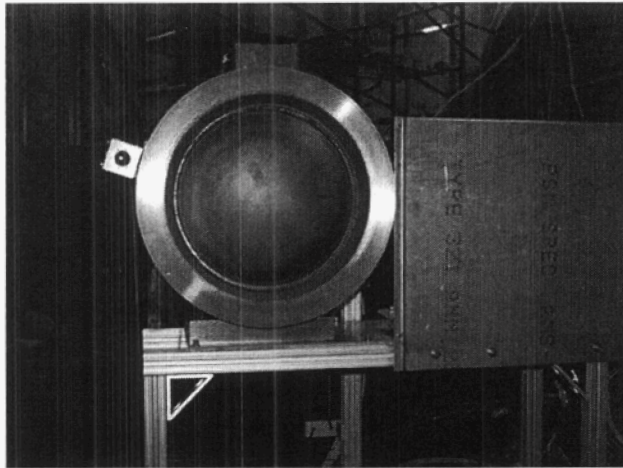


Figure 1. NKO Thruster in test facility



Figure 2. Vacuum Facility used to test FT2

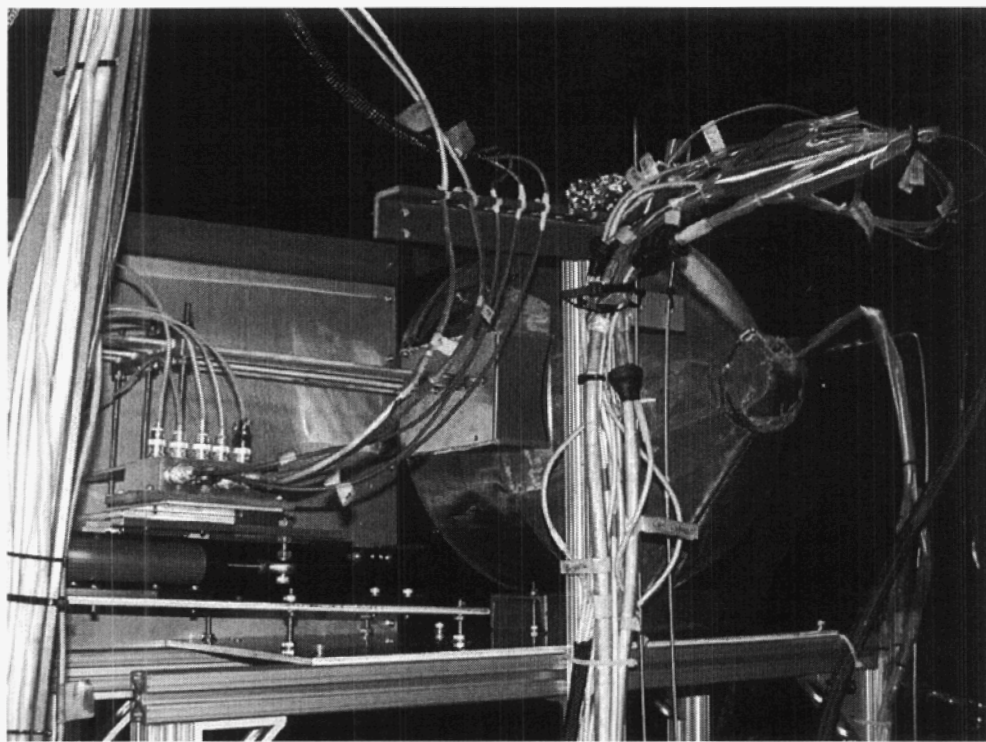


Figure 3. Rear view of the engine in test facility fitted with 7 probes

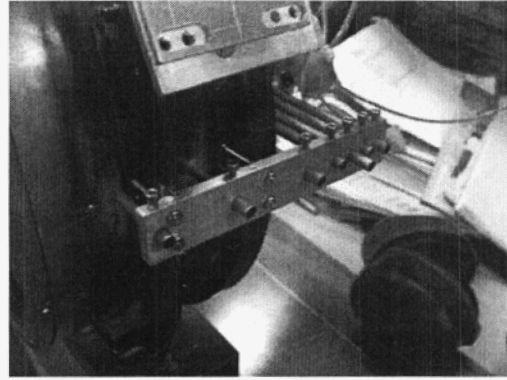
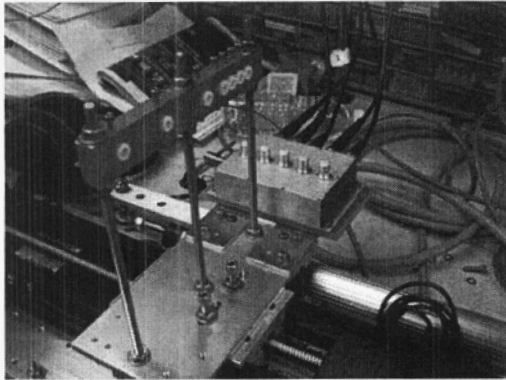


Figure 4. (a) Probe mount and electrical junction box, (b) thruster probe mount

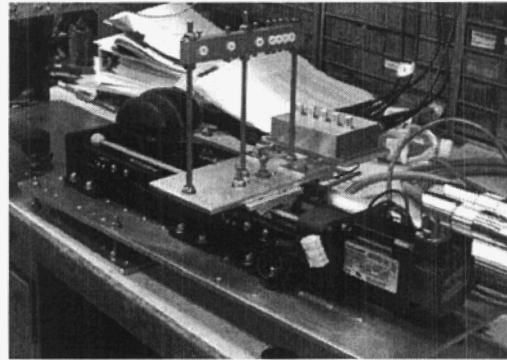


Figure 5. (a) ,Probe insertion into engine (b)Probe Translation Stage

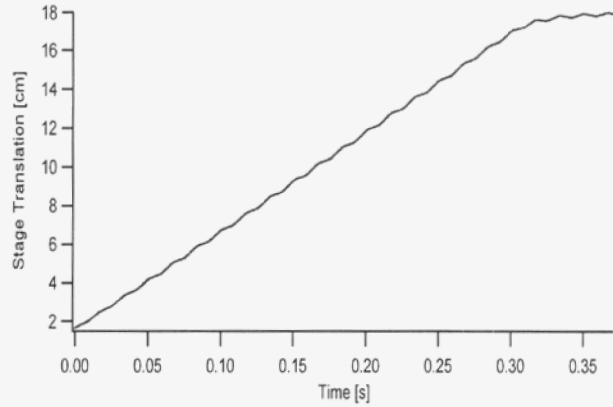
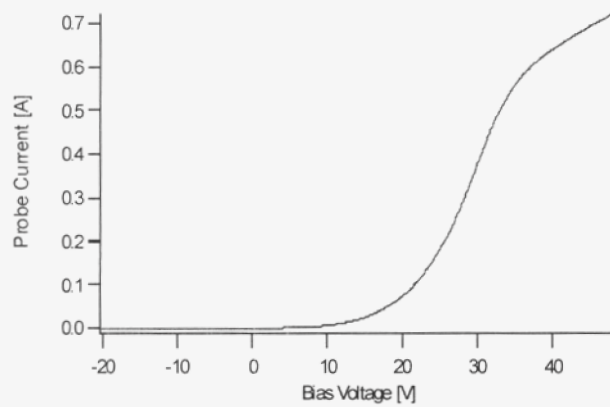


Figure 6. (a) Typical Probe IV Characteristic, (b) Linear position versus time for a single probe insertion

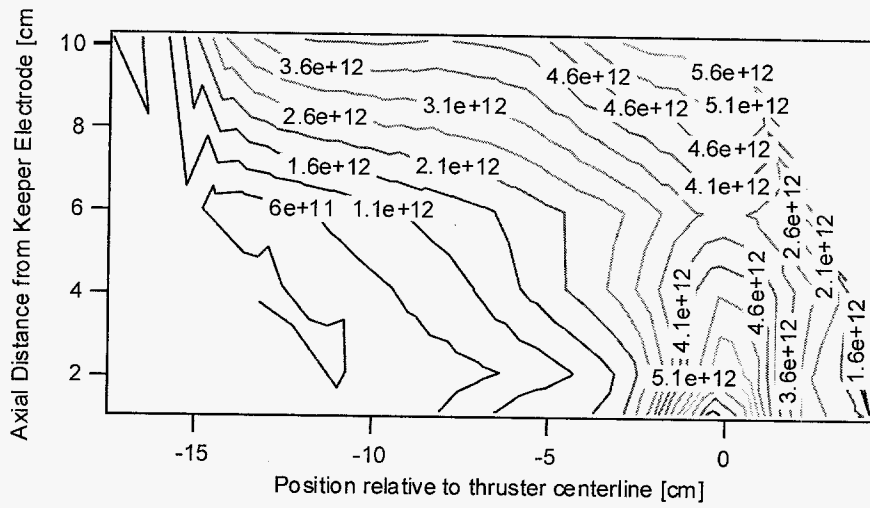


Figure 7. Electron Number Density at TH15 nominal operating point

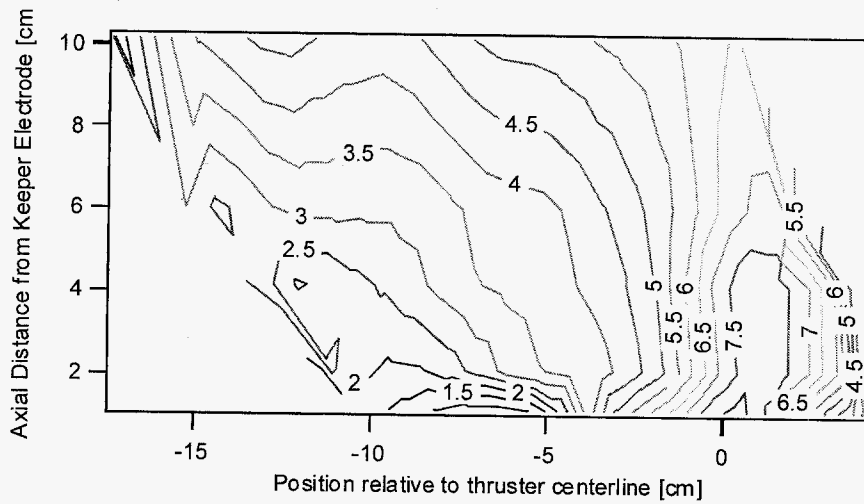


Figure 8. Electron Temperature at TH15 nominal operating point

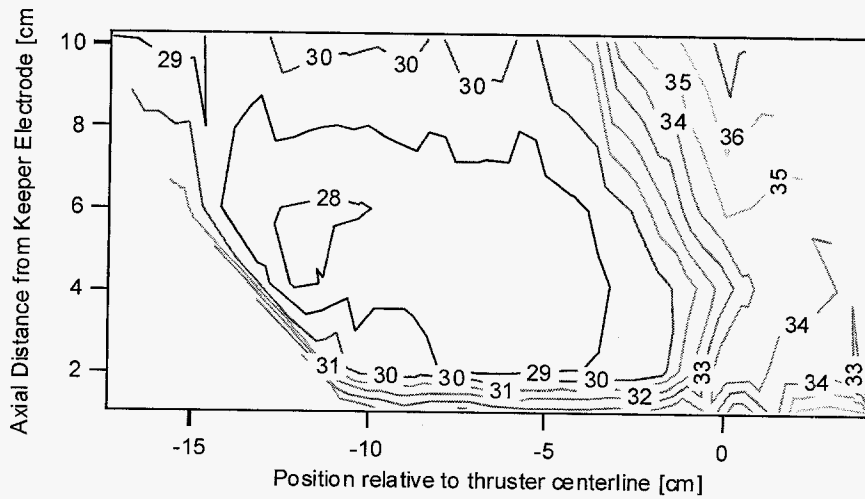


Figure 9. Plasma Potential with respect to Cathode Common at TH15 nominal operating point

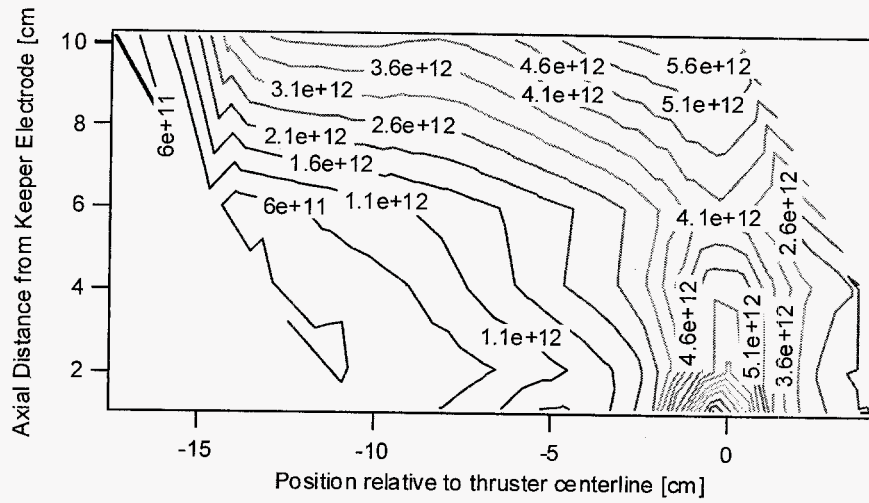


Figure 10. Electron Number Density at TH15 with -20% mc operating point

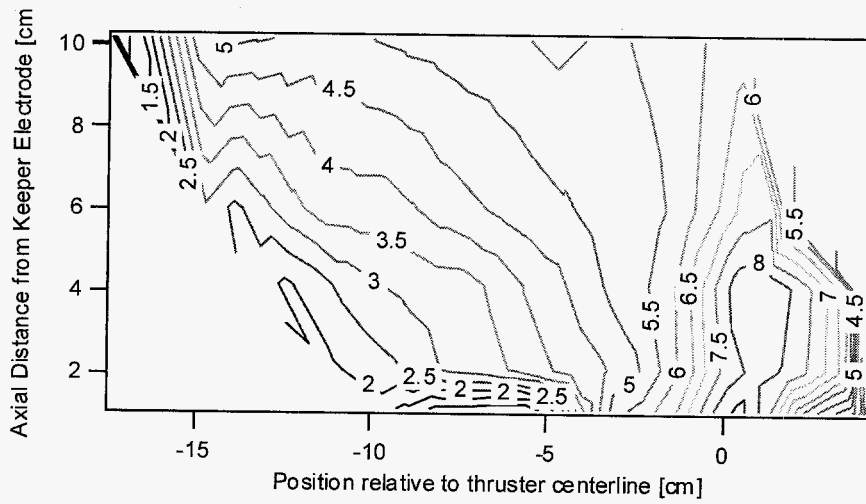


Figure 11. Electron Temperature at TH15 with -20% mc operating point

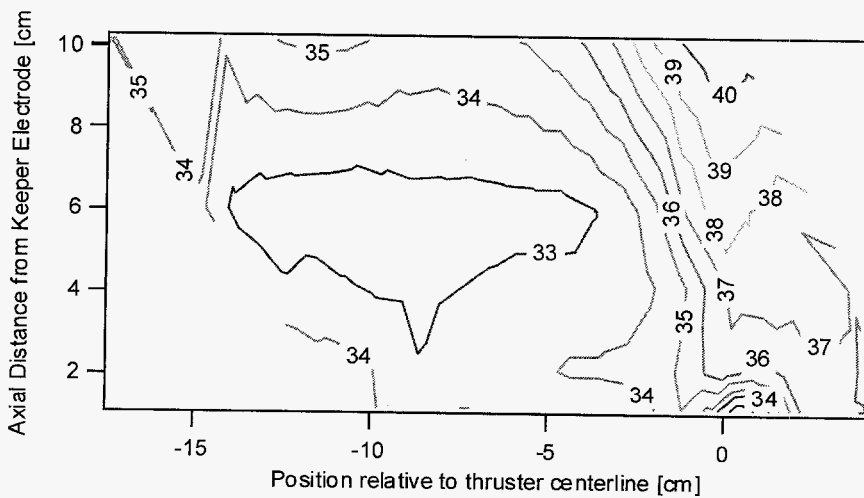


Figure 12. Plasma Potential with respect to Cathode Common at TH15 with -20% mc operating point

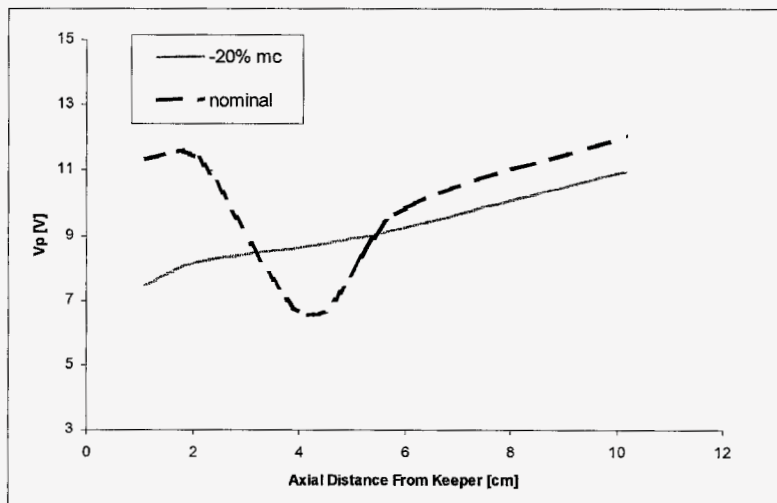
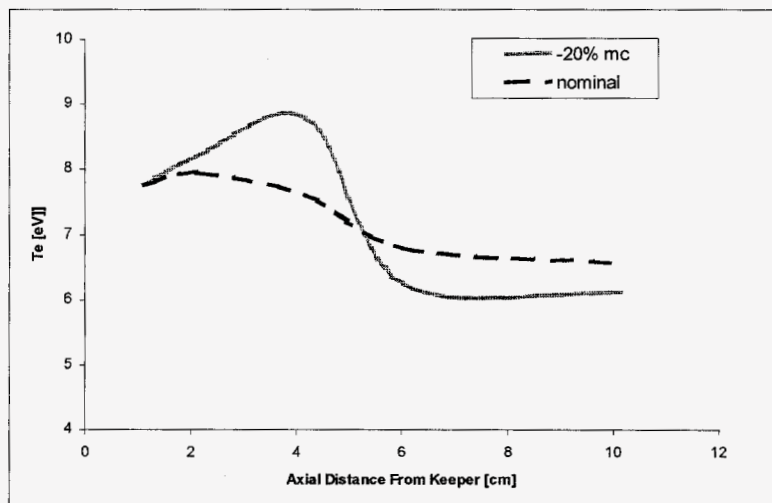
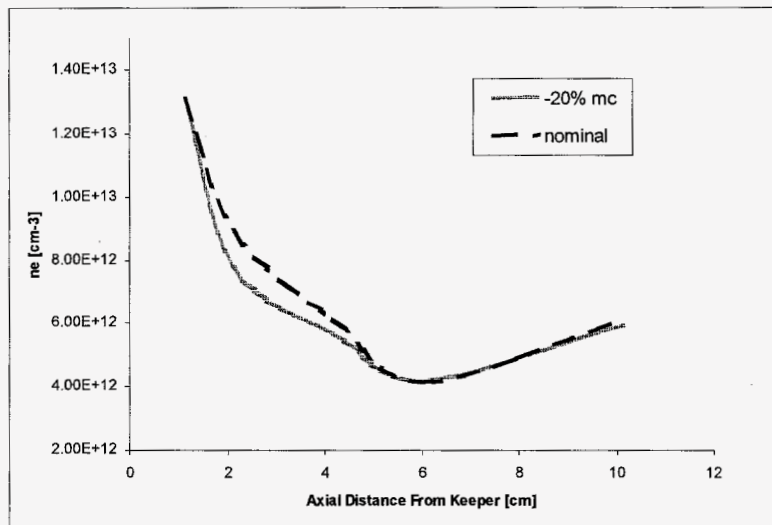


Figure 13. Electron number density, electron temperature, and plasma potential along the thruster centerline at operation point TH15 with nominal cathode flow rate and -20% of the nominal flow rate. Values are plotted as a function of axial distance from the discharge cathode keeper electrode.

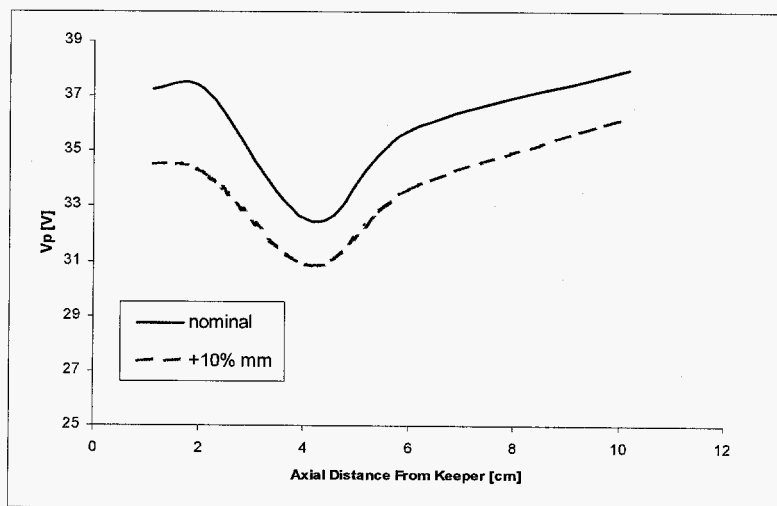
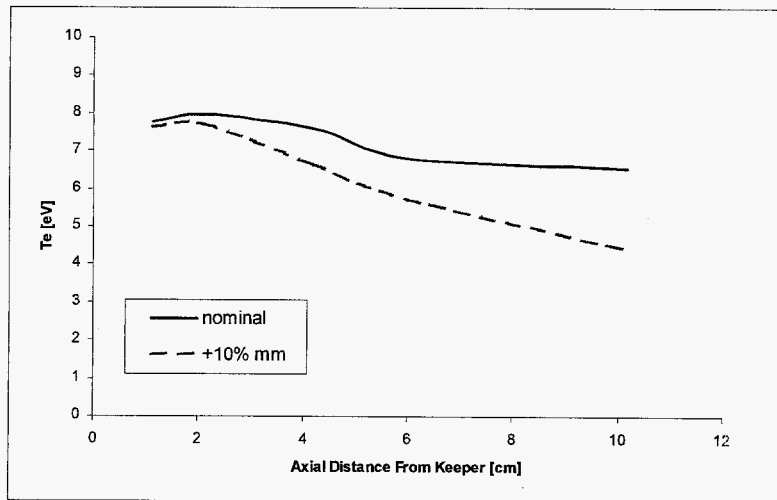
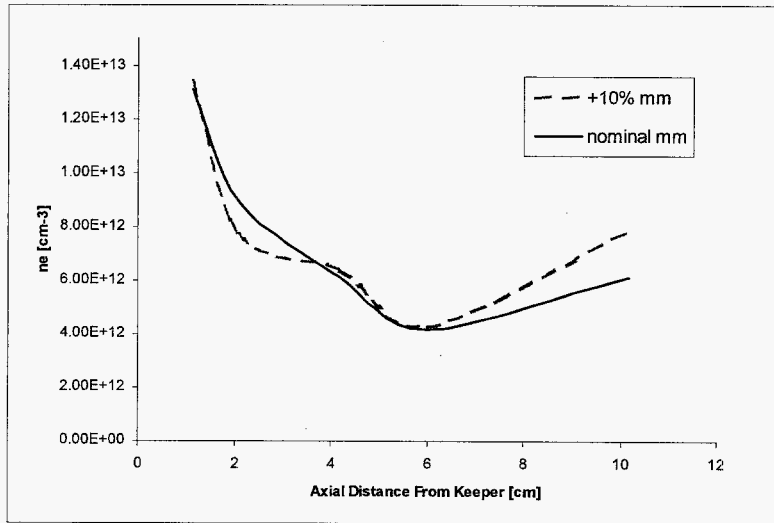


Figure 14. Electron number density, electron temperature, and plasma potential along the thruster centerline at operation point TH15 and with +10% of the nominal main flow rate. Values are plotted as a function of axial distance from the discharge cathode keeper electrode.

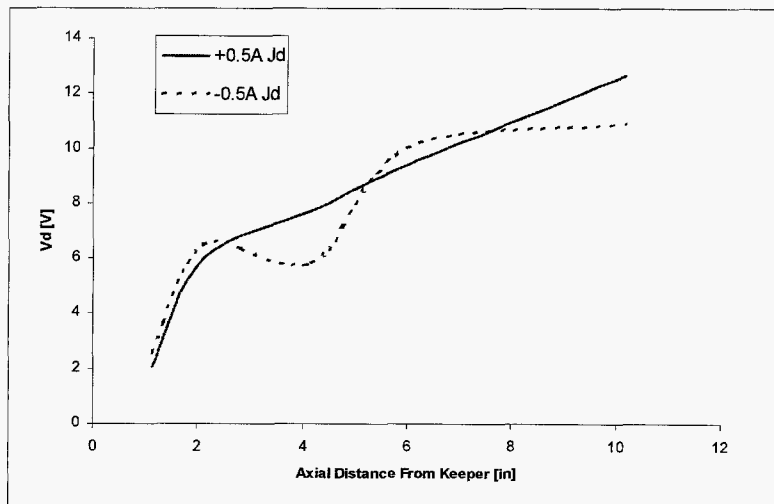
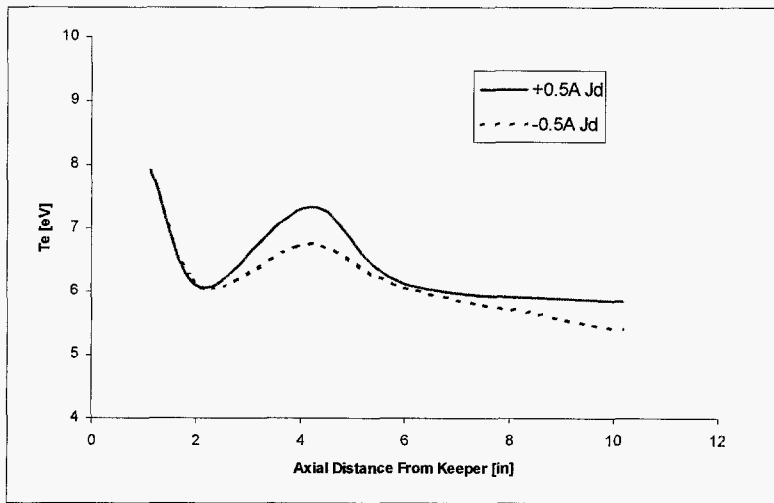
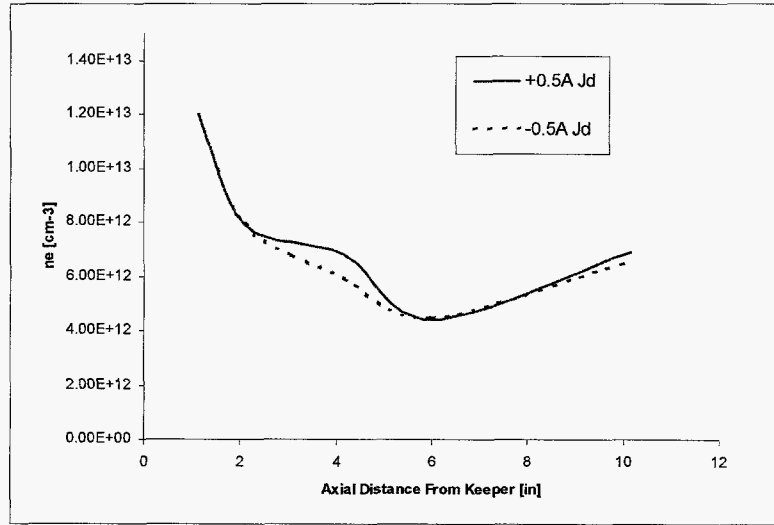


Figure 15. Electron number density, electron temperature, and plasma potential along the thruster centerline at operation point TH15 with $+0.5\text{A}$ and -0.5A from the nominal 15A . Values are plotted as a function of axial distance from the discharge cathode keeper electrode.

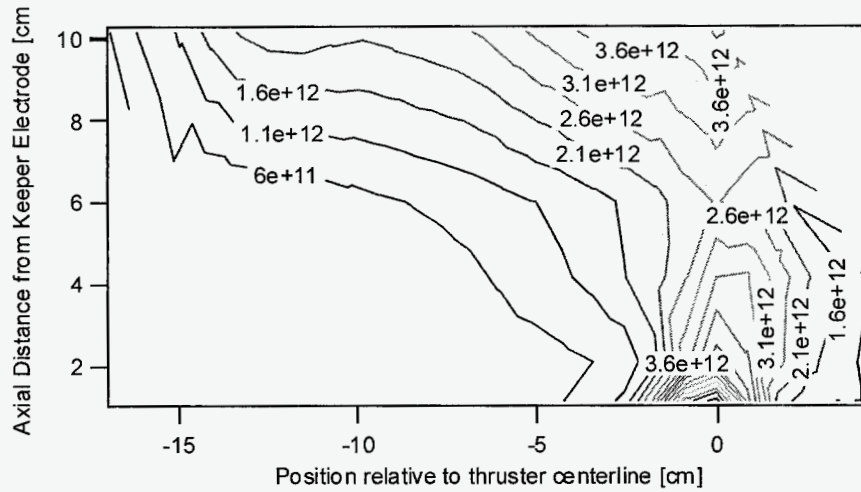


Figure 16. Electron Number Density at TH8 nominal operating point

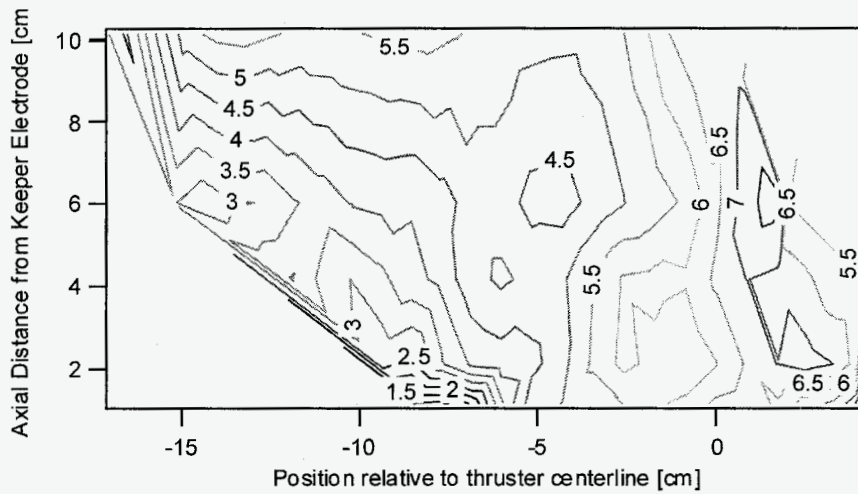


Figure 17. Electron Temperature at TH8 nominal operating point

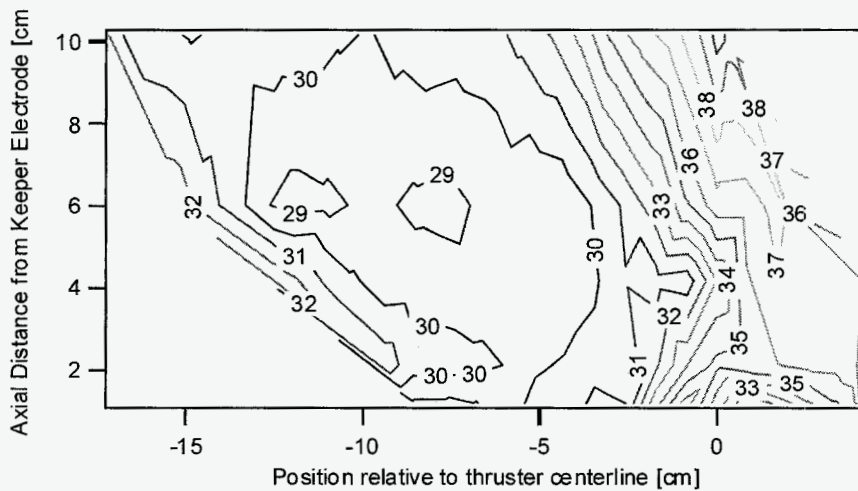


Figure 18. Plasma Potential with respect to Cathode Common at TH8 nominal operating point

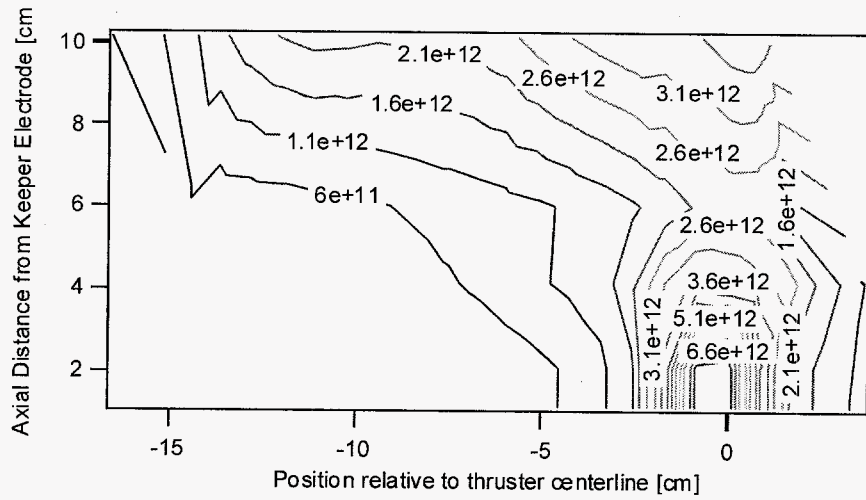


Figure 19. Electron Number Density at TH8 with -20% mc operating point

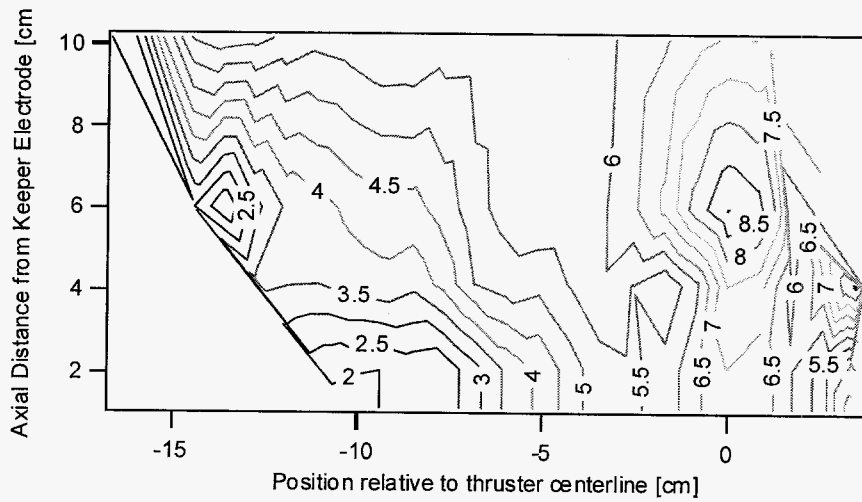


Figure 20. Electron Temperature at TH8 with -20% mc operating point

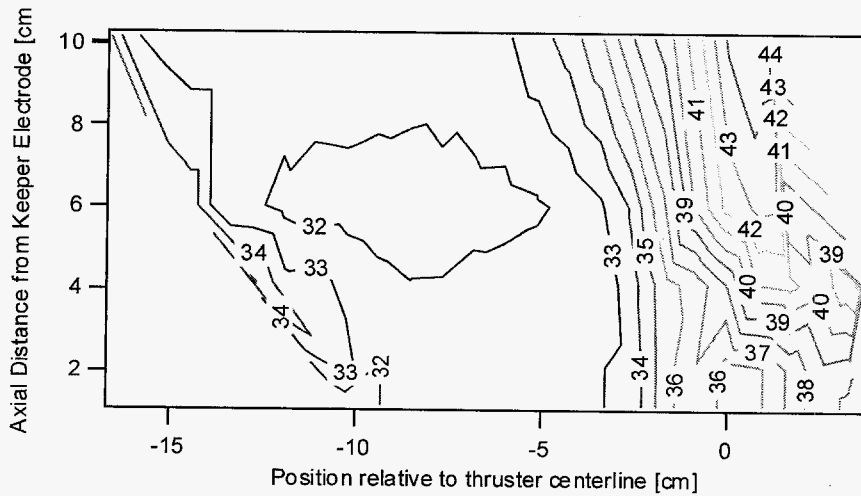


Figure 21. Plasma Potential with respect to Cathode Common at TH8 with -20% mc operating point

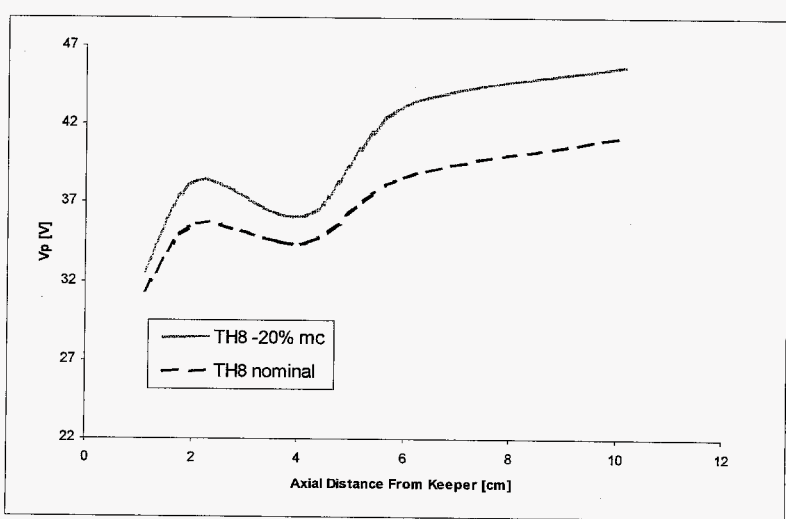
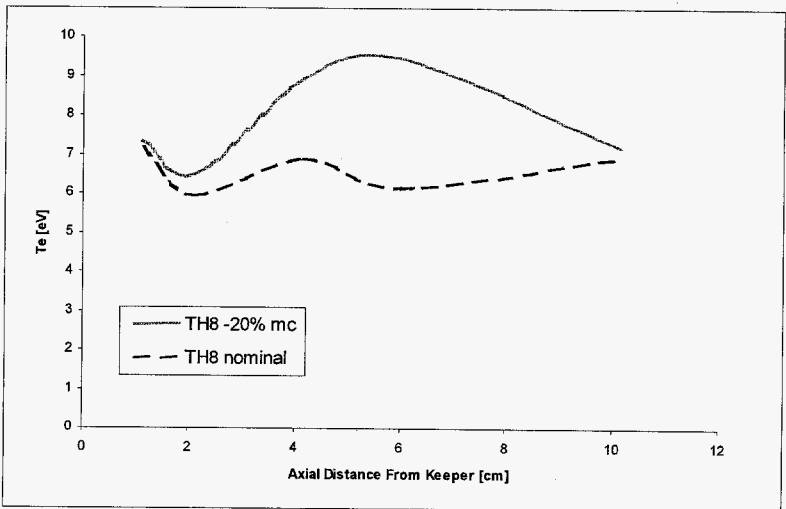
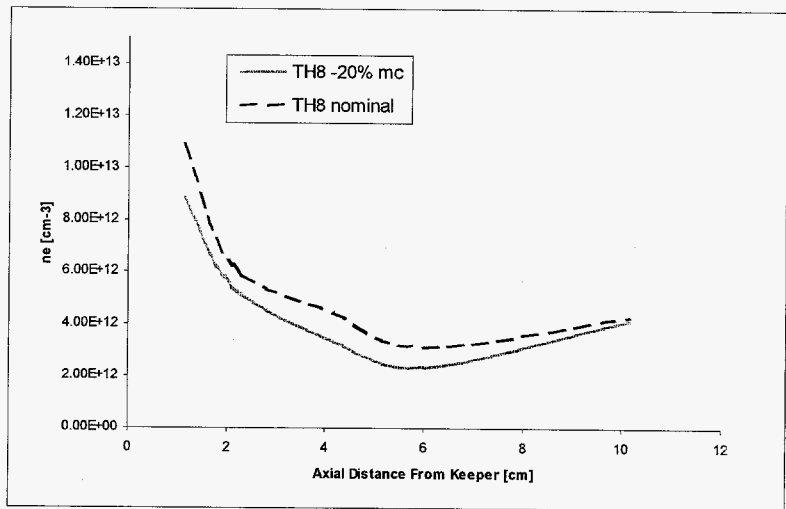


Figure 22. Electron number density, electron temperature, and plasma potential along the thruster centerline at operation point TH8 with nominal cathode flow rate and -20% of the nominal flow rate. Values are plotted as a function of axial distance from the discharge cathode keeper electrode.

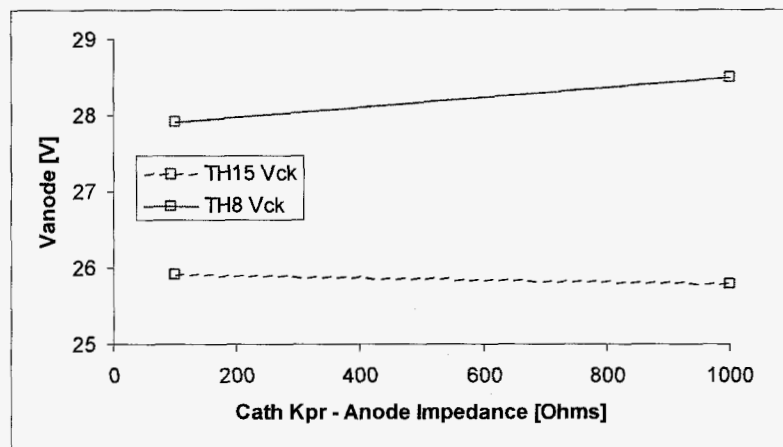
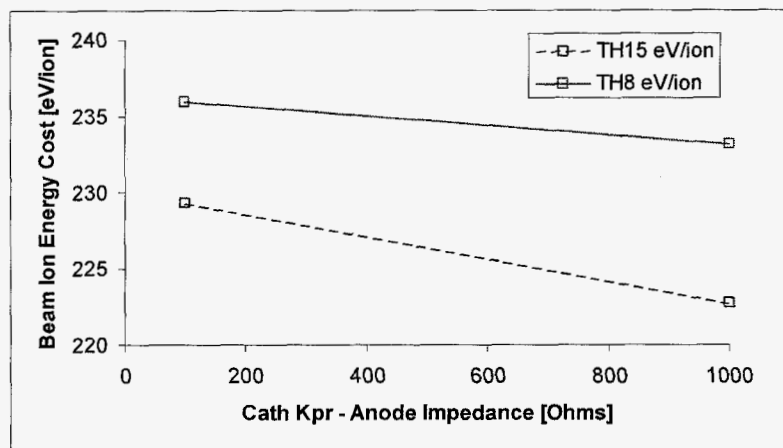
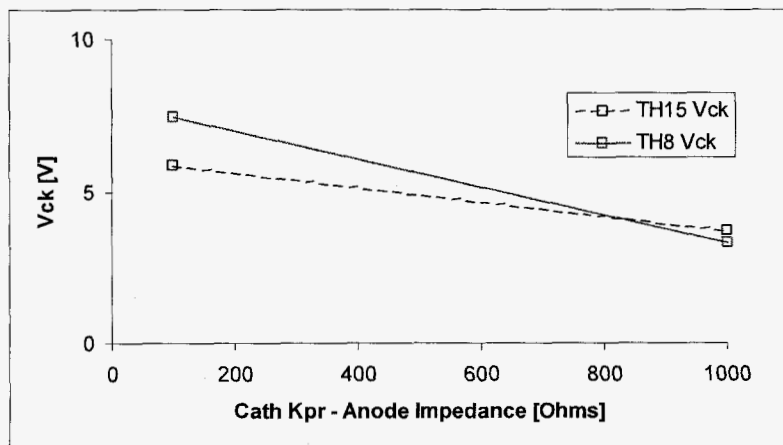


Figure 23. Cathode keeper to cathode common voltage, beam ion energy cost (discharge loss), and discharge voltage as a function of cathode keeper to anode resistance.

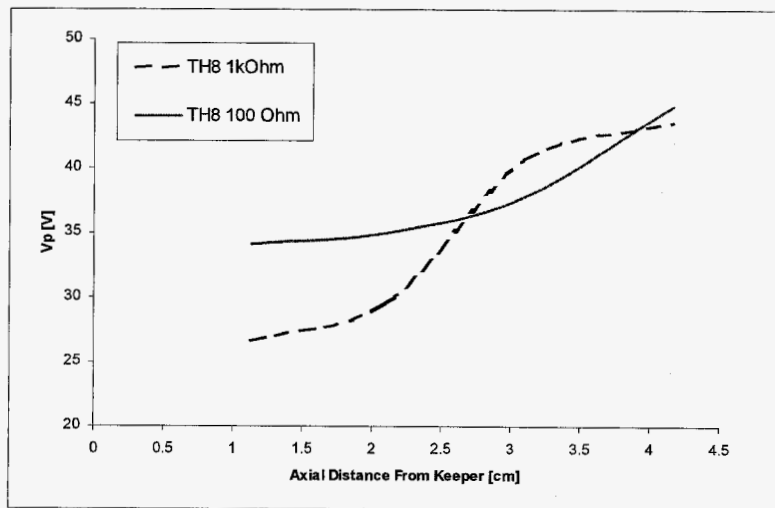
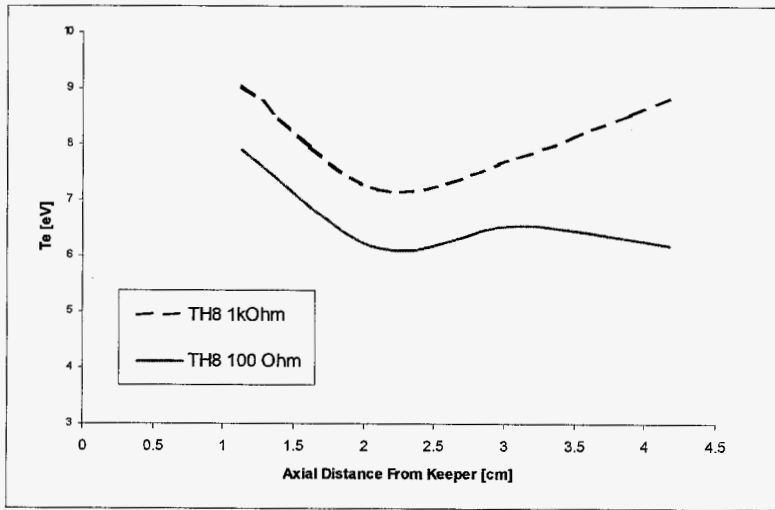
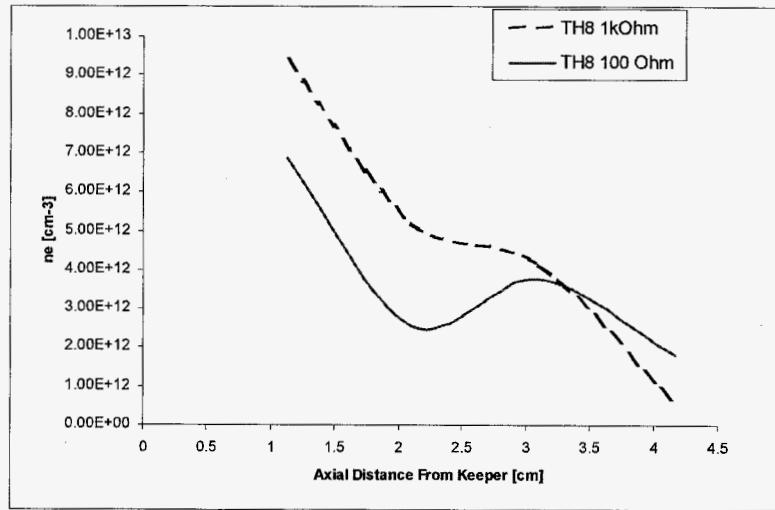


Figure 24. Electron number density, electron temperature, and plasma potential along the thruster centerline at operation point TH8 with 1k Ohm and 100 Ohm impedance between cathode keeper to anode. Values are plotted as a function of axial distance from the discharge cathode keeper electrode.

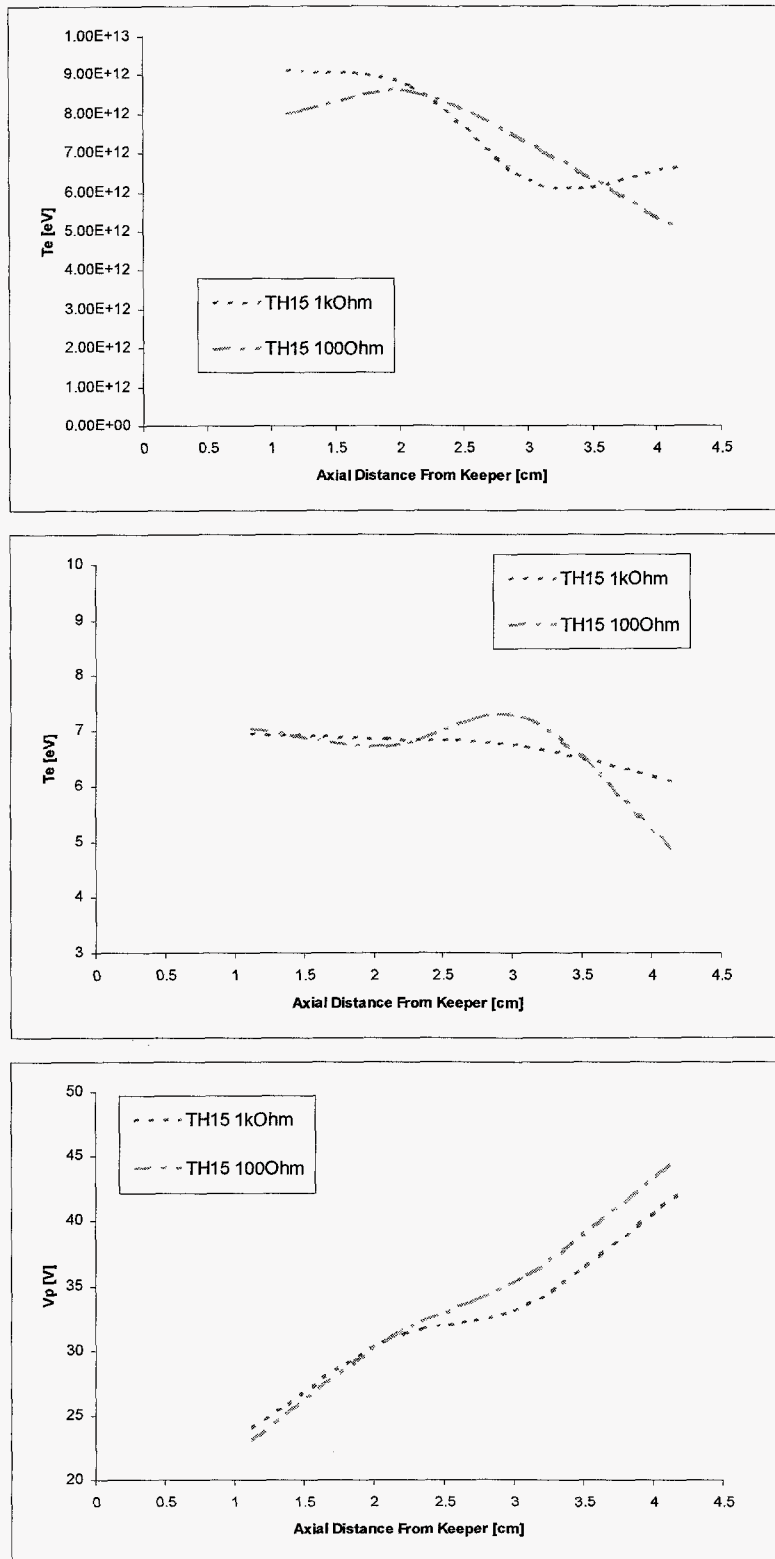


Figure 25. Electron number density, electron temperature, and plasma potential along the thruster centerline at operation point TH15 with 1k Ohm and 100 Ohm impedance between cathode keeper to anode. Values are plotted as a function of axial distance from the discharge cathode keeper electrode.

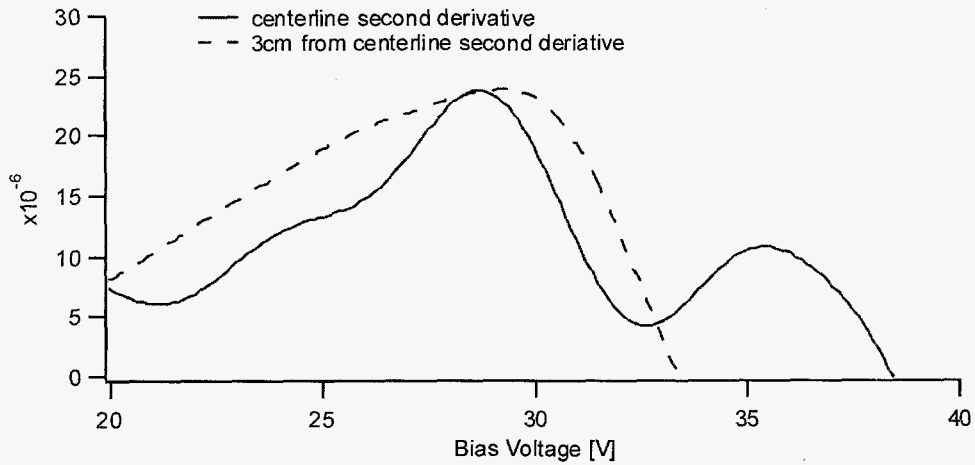


Figure 26. Second derivative of the electron retardation region of two different TH15 probe traces both located 4cm downstream of the cathode keeper, but at different radial locations.

NSTAR Throttle Level	Nominal Thruster Power	Beam Supply Voltage	Beam Current	Accelerator Grid Voltage	Neutralizer Keeper Current	Main Flow	Discharge Cathode Flow	Neutralizer Cathode Flow
	kW	V	A	V	A	sccm	sccm	sccm
TH 0	0.52	650	0.51	-150	2.0	5.98	2.47	2.40
TH 1	0.66	850	0.53	-150	2.0	5.82	2.47	2.40
TH 2	0.75	1100	0.52	-150	2.0	5.77	2.47	2.40
TH 3	0.91	1100	0.61	-150	2.0	6.85	2.47	2.40
TH 4	1.02	1100	0.71	-150	2.0	8.30	2.47	2.40
TH 5	1.12	1100	0.81	-150	2.0	9.82	2.47	2.40
TH 6	1.24	1100	0.91	-150	2.0	11.33	2.47	2.40
TH 7	1.34	1100	1.00	-150	2.0	12.90	2.47	2.40
TH 8	1.46	1100	1.10	-180	1.5	14.41	2.47	2.40
TH 9	1.58	1100	1.20	-180	1.5	15.98	2.47	2.40
TH10	1.72	1100	1.30	-180	1.5	17.22	2.56	2.49
TH11	1.85	1100	1.40	-180	1.5	18.51	2.72	2.65
TH12	1.96	1100	1.49	-180	1.5	19.86	2.89	2.81
TH13	2.08	1100	1.58	-180	1.5	20.95	3.06	2.98
TH14	2.20	1100	1.67	-180	1.5	22.19	3.35	3.26
TH15	2.33	1100	1.76	-180	1.5	23.43	3.70	3.60

Table 1. NSTAR Throttle table[3]

Figure X. Ion number density at TH15 and TH8 nominal operating points.

Figure X. Relative Neutral density profiles for TH15 as a function of axial distance from the cathode keeper electrode.